# The structure of a Tau fragment bound to tubulin prompts new hypotheses on Tau mechanism and oligomerization

Liza Ammar Khodja, Valérie Campanacci, Guy Lippens, Benoît Gigant

# The structure of a Tau fragment bound to tubulin prompts new hypotheses on Tau mechanism and oligomerization

Liza Ammar Khodja[1,§], Valérie Campanacci[1], Guy Lippens[2], Benoît Gigant[1,#]

[1] Université Paris-Saclay, CEA, CNRS, Institute for Integrative Biology of the Cell (I2BC), 91198, Gif-sur-Yvette, France.

[2] TBI, Université de Toulouse, CNRS, INRAE, INSA, 31077 Toulouse, France

[§] Present address. Laboratoire d'Ingénierie des Systèmes Macromoléculaires (LISM), Institut de Microbiologie, Bioénergies et Biotechnologie, Aix-Marseille Université-CNRS, UMR 7255, 13009 Marseille, France.

[#] Correspondence to benoit.gigant@i2bc.paris-saclay.fr (BG).

Keywords. Cytoskeleton; Microtubule dynamics; Structural biology; Tauopathies.

**Tau is a protein involved in the regulation of axonal microtubules in neurons. In pathological conditions, it forms filamentous aggregates which are molecular markers of neurodegenerative diseases known as tauopathies. Structures of Tau in fibrils or bound to the microtubule have been reported. We present here a structure of a Tau construct comprising the PHF6 motif, an oligopeptide involved in Tau aggregation, as a complex with tubulin. This Tau fragment binds as a dimer to a new site which, when transposed to the microtubule, would correspond to a pore between protofilaments. These results raise new hypotheses on Tau-induced microtubule assembly and stabilization and on Tau oligomerization.**

## Significance

Whereas the Tau protein is found aggregated in Alzheimer's disease and in related neurodegenerative disorders, in physiological conditions, it can bind in an elongated conformation along microtubules and regulates their dynamics. Using a fragment of Tau that is involved in its oligomerization, we identify a previously undescribed tubulin surface targeted by Tau, suggesting a dual binding mode. From these results, we formulate new hypotheses on the regulation of microtubules by Tau and on Tau oligomerization.

Tau is a microtubule-associated protein (MAP) that regulates microtubule dynamics in nerve cell axons (1). It is an intrinsically disordered protein which, in the adult human brain, exists as six isoforms resulting from alternative mRNA splicing (2), not to mention the little studied Big Tau variant (3, 4). Tau proteins are notably characterized by the presence of three or four microtubule binding repeats (MTBRs, named R1 to R4 hereafter), which are imperfect repetitions of a motif of 31 to 32 residues (5), defining 3R and 4R isoforms, respectively. In pathological conditions, Tau forms filamentous aggregates, which are molecular markers of neurodegenerative diseases called tauopathies (6). In these aggregates, part of the MTBR region and a short extension C-terminal to it adopt β-strand rich, disease-specific molecular conformers, which have led to a structure-based classification of tauopathies (7). Similar structural diversity is observed in filaments assembled in vitro from recombinant Tau (8).

Diversity is a term that also applies to the association of Tau with microtubules. Indeed, Tau decorates microtubules in a non-uniform way (9), and small oligomers of 2 to 3 molecules (10), medium-size patches comprising 3 to 20 molecules (11), or unsaturable clusters (12) forming envelopes around microtubules (13, 14) have been reported. Tau also partitions between populations of molecules which either are in rapid equilibrium with, or dissociate very slowly from microtubules (15, 16). These results echo experiments showing that some of the Tau molecules diffuse on microtubules whereas others are static (17). Relatedly, different interaction modes of Tau have been postulated (18–23) but only a binding of the MTBR region in an extended conformation along protofilaments, at the outer surface of the microtubule, has been firmly established (24). The most obvious mechanism that can be inferred from these last results is that Tau strengthens longitudinal contacts, i.e. between tubulins along a protofilament, to favor microtubule assembly and stabilization (24), potentially by preventing the dissociation of tubulin at microtubule ends (16). Experimental evidence for enhanced longitudinal interactions, but also for an alternative mechanism consisting in reinforcing lateral contacts (between protofilaments), is however scarce (25).

Not unexpectedly for a protein that favors microtubule assembly, Tau also binds to soluble tubulin, the interaction with both partners displaying similarities (26, 27). In particular, in both cases, the association leads to dynamic complexes (21, 23, 28, 29). To characterize the mechanism of Tau further, we determined a Tau:tubulin structure and identified a binding site for the 3$^{rd}$ MTBR (R3). When modeled on the microtubule, this repeat would bind as a dimer to a pore at the corner of four tubulin molecules from two protofilaments. The implications of this model for the mechanism of microtubule regulation by Tau and its potential connection with Tau oligomerization are discussed.

## Results and Discussion

### Structure of Tau R3 bound to tubulin

The interaction of Tau with microtubules has been studied by cryo-EM, leading to structural models for the binding of the 1st and 2nd MTBR (24). By contrast, studies of the interaction with soluble tubulin have defined the association as dynamic and heterogenous (23, 27, 30) but high resolution data were missing. Our first efforts to crystallize such a complex, using Tau constructs added to tubulin bound to different crystallization helper proteins (31), were unsuccessful. To facilitate the crystallization process, and using the R2-decorated microtubule cryo-EM model as a guide (24), we designed the D2-R3 fusion protein in which a Tau fragment was linked to the C-terminus of D2ΔC, a tubulin-specific Designed Ankyrin Repeat Protein (DARPin) (32) devoid of its C-terminal α-helix (see Methods and Fig. S1). D2-R3 includes residues 302 to 324 of Tau, therefore mainly from the R3 repeat (numbering is according to the Tau441 isoform). Spanning the sequence that produces the shared first intermediate amyloid filament between Alzheimer's disease and chronic traumatic encephalopathy filaments (33), it comprises in particular the $^{306}$VQIVYK$^{311}$ PHF6 peptide, thought to be a nucleus of Tau aggregation (34). For crystallization, a stathmin-like domain protein (hereafter named SLD1) engineered to bind a single αβ-tubulin heterodimer (32) was further added to tubulin:D2-R3. Molecular replacement allowed us to place two SLD1:tubulin:D2ΔC complexes in the asymmetric unit. In addition, we identified an electron density signal in which we could build two parallel β-strand-like polypeptide stretches that we attributed to Tau R3, which therefore binds as a dimer (Fig. S2).

Inspection of the crystal packing indicated that the C-termini of the two DARPins of the asymmetric unit are, as expected, in the vicinity of the N-termini of the R3 stretches. Interestingly, it is also the case for the C-termini of the two SLD1 molecules (Fig. S2). This feature prompted us to graft the R3 fragment to SLD1 and produce an SLD1-R3 chimera. We then determined the structure of SLD1-R3:tubulin, this time using the D2ΔC DARPin as a crystallization helper. As above, an electron density signal attributed to Tau R3 was present, indicating that the binding of R3 to tubulin does not depend on what protein, either D2ΔC or SLD1, it is fused to. In these two structures, the signal for Tau R3 was however substantially weaker than that of tubulin, which can be illustrated for instance by comparing temperature factors (Table 1). This lower signal may reflect a molecular mobility of Tau in the complex, but it can also result from a lower occupancy of the Tau part, either because of constraints imposed by the chimeric constructs or because of an affinity issue. Indeed, short constructs of

Tau have been shown to bind only weakly to microtubules or tubulin (26, 29, 35, 36). In an attempt to increase the occupancy, we crystallized tubulin in complex with D2-R3 and SLD1-R3, i.e. with the Tau fragment fused to both D2ΔC and SLD1, and obtained data up to 2.2 Å resolution (Table S1; Fig. 1A). Although still lower than that of tubulin, the signal for the Tau peptide dimer was improved (Table 1; Fig. 1B and S3) and this structure was used for the analysis presented in this manuscript.

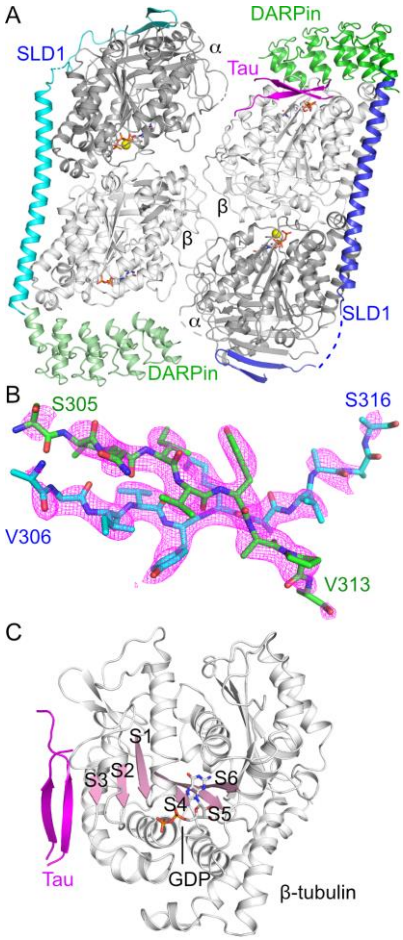


**Figure 1**. Structure of Tau R3 bound to tubulin. (A) Asymmetric unit content of the SLD1-R3:tubulin:D2-R3 crystals. The α- and β-tubulin subunits are in dark and light grey, respectively, SLD1 molecules in cyan or blue, and the DARPins in two shades of green. Tau R3 is in magenta. (B) Section of a 2 $F_{obs}$-$F_{calc}$ composite electron density omit map contoured at the 1 σ level and centered on the Tau R3 stretches. The side chains of residues Val306, Gln307, Asp314, Leu315 and Ser316 of the stretch closest to tubulin (cyan) and of Lys311 and Val313 of the second stretch (green), which are weakly defined in the electron density maps, have been truncated after their Cβ atom. (C) The two parallel β-strand R3 stretches (magenta) extend the β-sheet (pink) of the β-tubulin N-terminal domain.

**Table 1.** Mean temperature factors of the Cαs of protein subunits in different tubulin:Tau R3 structures [(a)].

| | SLD1:tubulin:D2-R3 | SLD1-R3: tubulin:D2ΔC | SLD1-R3:tubulin: D2-R3 |
|---|---|---|---|
| Resolution | 2.13 Å | 2.0 Å | 2.21 Å |
| α-tubulin (chain A) | 71 Å$^2$ (413) [(b)] | 61 Å$^2$ (422) | 57 Å$^2$ (426) |
| α-tubulin (chain E) | 65 Å$^2$ (426) | 63 Å$^2$ (427) | 48 Å$^2$ (427) |
| β-tubulin (chain B) | 36 Å$^2$ (433) | 32 Å$^2$ (432) | 27 Å$^2$ (432) |
| β-tubulin (chain F) [(c)] | 37 Å$^2$ (432) | 33 Å$^2$ (431) | 29 Å$^2$ (435) |
| Tau R3 | 87 Å$^2$ (17) | 106 Å$^2$ (17) | 67 Å$^2$ (20) |

[(a)] All data were processed and the structures refined as described for SLD1-R3:tubulin:D2-R3. [(b)] Values in parentheses are the number of Cα atoms of the residues drawn in the model. [(c)] β-tubulin subunit in interaction with the Tau R3 stretches.

Residues Ile308 to Val313 of the strand closest to tubulin and residues Val306 to Pro312 of the second one could be built in the initial electron density "omit" maps following molecular replacement (Fig. S3). The side chains were reasonably defined except that of Lys311 in the second strand. During refinement, we were able to extend this initial model and include residues 306 to 316 and 305 to 313 of the first and second Tau stretches, respectively, but only the main chain was traced for most of these additional residues (Fig. 1B). These two parallel PHF6 β-strands, with the side chains of both Tyr310 residues pointing in opposite direction, adopt yet another conformations compared to those described in different fibrillar structures (37), possibly because they extend the β-sheet of the N-terminal domain of the β-tubulin subunit they interact with (Fig. 1C). Incidentally, the same sequence of the interacting S3 β-strand on the tubulin side ($^{91}$NFVFGQ$^{96}$) is also found in a phosphate-binding protein from *Stenotrophomonas maltophilia* (pdb id 5J1D and 5JK4) where it adopts a β-strand that is extended by a LVQI peptide in an antiparallel β-sheet conformation, reminiscent of our present R3:tubulin model (Fig. S4). Importantly, this binding mode of Tau R3 to tubulin (Fig. 1) is different from that planned when designing D2-R3 (Fig. S1A) and was made possible by the symmetry of the crystal (Fig. S2).

**A binding specific to the R3 repeat?**

We then asked whether the other Tau MTBRs can bind to tubulin in the same way as R3. This hypothesis seems reasonable at least in the case of R2 because this repeat includes the PHF6* $^{275}$VQIINK$^{280}$ hexapeptide related to the R3 PHF6 (Fig. S1C). To this end, we crystallized SLD1:tubulin further complexed with constructs analogous to D2-R3 but in which the R3 MTBR part was replaced by that of R1 (D2-R1), R2 (D2-R2) or R4 (D2-R4) (Fig. S1D). We also obtained SLD1-R2:tubulin:D2ΔC crystals, i.e. with the R2 fragment fused to SLD1.

However, in none of these cases, electron density signal overlapping with that attributed to Tau R3 was present. Therefore, this result provides additional indication that the two hexapeptide motifs are not equivalent. Indeed, it has been observed that the PHF6 has a stronger effect on microtubule stabilization than the PHF6* (38), and the aggregation tendency of the former is also stronger than for PHF6* (39), a feature related to the nature of the residue, either a serine or a lysine, just N-terminal to the hexapeptide (40). To summarize, our results suggest a binding to tubulin specific to the R3 repeat of Tau.

**A model of R3 bound to microtubules and its implications**

In the crystal, the two R3 stretches are sandwiched between two β-tubulin subunits (Fig. S2E-G), reminiscent of an inter-protofilament environment (Fig. 2A). Accordingly, if we superimpose the structure of β-tubulin of SLD1-R3:tubulin:D2-R3 to that of β-tubulin in a microtubule (41), the accompanying Tau R3 stretches occupy a microtubule pore, at the interface of four tubulin heterodimers from two protofilaments (Fig. 2B). Therefore, the binding of the 3rd repeat of Tau to tubulin (Fig. 1A) leads, when transposed to the microtubule, to a model distinct from the binding of R1 and R2 MTBRs at the crest of a protofilament (24) (Fig. 2B).

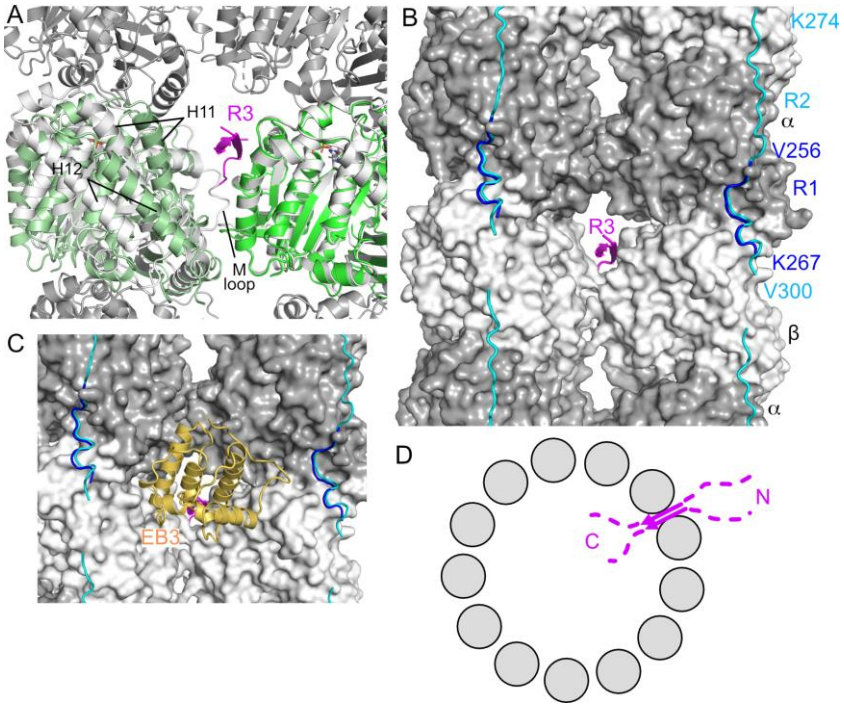


**Figure 2**. Model of Tau R3 bound to microtubules. (A) In the crystal, the R3 stretches are sandwiched between two β-tubulin subunits arranged as in adjacent protofilaments. The β-tubulin subunit of SLD1-R3:tubulin:D2-R3 in contact with the Tau fragment (β-tubulin in

bright green, with the accompanying Tau R3 stretches in magenta) has been superimposed to a β-tubulin subunit of the microtubule (pdb id 6DPU; β-tubulin in light grey, α-tubulin in darker grey). A crystal-related β subunit is shown in light green. Its C-terminal H11 and H12 helices, as well as those of β-tubulin (and its M-loop) of an adjacent protofilament in the microtubule, are labeled. (B) Model of Tau R3 targeting a microtubule pore formed by four tubulin heterodimers from two protofilaments. β-tubulin of SLD1-R3:tubulin:D2-R3 has been superimposed to a β subunit of the microtubule as in panel A (view from the outside of the microtubule, with the plus end at the top of the figure; two protofilaments are drawn). Only the Tau part of SLD1-R3:tubulin:D2-R3 is shown (magenta). R1 and R2 MTBRs bound along the crest of the protofilaments in the structure of Tau-decorated microtubules (pdb id 6CVJ and 6CVN, respectively, with the limits of the fragments drawn in the cryo-EM maps indicated at the top, right of the figure) are also shown (in blue and cyan, respectively). (C) The binding site of R3 modeled on the microtubule overlaps with that of the EB3 calponin-homology domain (pdb id 3JAR). (D) Schematic drawing of two Tau molecules trapped between protofilaments of the microtubule. The model of the R3 PHF6 dimer targeting a hole between protofilaments implies that the N-terminal and C-terminal regions of Tau would be outside and inside the microtubule, respectively.

The microtubule binding site of Tau R3 suggested by this modeling would account for previous results and analyses. For instance, two binding modes of Tau to microtubules have been deduced from kinetic studies using fluorescently-labeled Tau molecules in vitro (15) or in cells (9). When Tau is added to preformed microtubules, a rapid association-dissociation kinetics was observed. When it is co-assembled with tubulin, in addition, a fraction of Tau molecules was found to be tightly bound and could not be displaced by Tau added afterwards (15). Tau molecules bound along protofilaments (24) might correspond to the species in rapid equilibrium (16) and might also correspond to the fraction of Tau able to diffuse along microtubules (17). Conceptually, however, a binding of the R3 MTBR at a microtubule pore would lead to Tau molecules trapped between protofilaments. Only possible if coupled with tubulin assembly, and emulating irreversible binding unless microtubules disassemble, such a binding mode would hence occur more frequently in the labile part of microtubules, where Tau is found to accumulate (42). Moreover, a binding site at the microtubule pore overlaps with those of EB proteins (41, 43) (Fig. 2C) and of doublecortin (44), which would contribute to the reported competition for microtubule binding between Tau and these proteins in cells (45–47). This

"second" binding site would also agree both with the flexural rigidity of microtubules which is enhanced by Tau only when it is added in a co-assembly manner but not when added to taxol-stabilized microtubules (48), and with the targeting of molecules to the lumen of the microtubule by a peptide spanning the PHF6 motif only when it is added before microtubule assembly (49).

In addition, it has been advocated that Tau can regulate microtubule dynamics by targeting either longitudinal or lateral contacts, but with little direct evidence (22, 23, 25, 50). Two R3 repeats bridging adjacent protofilaments through a Tau:Tau interaction would strengthen lateral interactions and could act in synergy with Tau molecules bound along protofilaments to foster longitudinal ones. In particular, reinforcing lateral contacts is expected to prevent protofilament peeling, typical for disassembling microtubules (51), giving a rationale for the stabilizing effect and inhibition of microtubule disassembly that has been observed at low Tau concentration (52), in agreement with cell experiments where Tau hotspots are found at microtubule ends during rescue and pause transitions (9). Interestingly, interfering with microtubule disassembly is a distinguishing property of 4R Tau compared to 3R isoforms (53). Because of the major contribution of the first repeat to the binding affinity for microtubule (29), Tau likely engages first its R1 repeat in the interaction with tubulin. Then, the other MTBRs may bind along the protofilament crest as observed by cryo-EM (24). Occasionally, R2 might not bind but give the flexibility needed for the PHF6 peptide at the start of R3 to target the tubulin surface identified in our X-ray structure. This scheme is only possible with 4R Tau, but not with 3R isoforms which are devoid of the 2$^{nd}$ MTBR (corresponding to residues Val275 to Ser305 in Tau441 (2)) and where R1 immediately precedes the PHF6 peptide. Indeed, when R1 along the protofilament ridge and R3 in the pore are modeled on the same microtubule (Fig. 2B), the closest distance between the Cαs of Lys267 (from R1) and of Val306 is about 37 Å. Therefore, simultaneous tight binding from the same 3R-Tau molecule of R1 along a protofilament and R3 between protofilaments would require a substantial structural rearrangement. In the case of 4R Tau, structural flexibility of the least contributing R2 repeat (29) might give the necessary slack for simultaneous binding of the R1 and R3 repeats along the two binding modes described.

Our model of R3 on microtubules also prompts new hypotheses regarding microtubule-induced Tau oligomerization. The most obvious one is related to the formation on microtubules of small patches of Tau, which can be composed of as few as two molecules (10). An oriented binding of the R3 repeats between protofilaments, with their C-terminal end pointing inside the microtubule (Fig. 2B,D), implies that the ~125 C-terminal residues of Tau would lie in the microtubule lumen, whereas its N-terminal region would be accessible at the exterior of the

microtubule. In addition, as mentioned above, a very slow dissociation would be expected for Tau bound in this mode unless the microtubule disassembles. Therefore, these patches would represent anchoring points for accumulation of additional Tau molecules that could lead to envelope formation on microtubules (13, 14). This hypothesis is consistent with the N-terminal part of Tau being involved in its oligomerization (13, 54, 55), and with Tau envelopes that have been dissolved by 1,6-hexanediol treatment re-forming at the same locations on the microtubule (14).

Another remarkable observation is that the N-termini of the ordered R3 stretches in our structure, at the beginning of the PHF6 peptide, correspond to that of the ordered core of filaments from Alzheimer's disease (56). These R3 stretches are already comprised in the first filamentous intermediates of Tau assembly into Alzheimer's disease and chronic traumatic encephalopathy filaments (33), but do not represent the start of fibrils in single Tau isoform diseases such as Pick's disease (3R tauopathy) (57) or corticobasal degeneration (4R tauopathy) (58). At present, our structure however cannot decide whether it results from an isoform-specific Tau:microtubule interaction or not (59).

In conclusion, we have identified a binding site for the R3 repeat of Tau to tubulin that differs from that of R1 and R2 to microtubules. Our results lead to a conceptual model of a dimer of Tau targeting a microtubule pore between protofilaments, with β-strand-type PHF6:PHF6 interactions that are reminiscent of those found in Tau aggregation (7, 34, 56). Whereas attractive, the extent to which this binding mode contributes to the mechanisms of Tau regulating microtubule dynamics or of its own oligomerization, be it physiological or pathological, remains to be evaluated.

## Methods

**Design of D2-R3 and other fusion proteins**. To enhance the likelihood to obtain a Tau:tubulin structure, we designed a chimera between a tubulin-binding DARPin protein (32, 60) and a Tau fragment. Such a fusion protein approach has been used to crystallize complexes of low affinity (61) or prone to form heterogenous aggregates (62, 63). Indeed, Tau:tubulin complexes may precipitate at high concentration (23). In addition, small fragments of Tau have a low affinity for microtubules or tubulin (26, 29, 35, 36). To build the D2-R3 fusion protein between D2 DARPin and Tau R3, this Tau repeat was modeled on tubulin:D2 (pdb id 4F6R) (32) using as a guide the cryo-EM model of R2 bound to the microtubule (pdb id 6CVN) (24) (Fig. S1A). To minimize the length of the linker between the two partners, the C-terminal helix of the DARPin

was removed (this C-terminal truncated DARPin was named D2ΔC). In addition, the length of the Tau fragment was optimized for this one-tubulin assembly. The final construct comprises residues 1-157 of the DARPin (hence residues 158-169 were omitted), a linker made of two $G_4S$ repeats and residues 302 to 324 of Tau (Fig. S1B). D2-R1, D2-R2 and D2-R4 were designed based on D2-R3, replacing the R3 moiety by the equivalent part of R1, R2 or R4, respectively (Fig. S1D). SLD1-R2 and SLD1-R3 were built using two $G_4S$ repeats to link the C-terminus of SLD1 to Tau residues Gly271 to Ser293 or residues Gly302 to Ser324, respectively. SLD1, originally named R1 (32), has been renamed here to avoid confusion with the Tau R1 repeat. All constructs were verified by sequencing.

**Protein purification**. D2-R3 was overexpressed in *Escherichia coli* and purified following the protocol of the parental D2 DARPin (32, 60). Briefly, it was expressed in XL1-Blue cells grown in 2YT medium after induction with 0.5 mM isopropyl β-D-1-thiogalactopyranoside for 4 h at 37°C. After sonication of the bacteria suspension, D2-R3 was purified from the soluble fraction by $Ni^{2+}$-affinity chromatography (Histrap HP, Cytiva) followed by gel filtration (Superdex 75 16/60 HL, Cytiva) in 20 mM Hepes-K, pH 7.2, 1 mM $MgCl_2$, 0.5 mM EGTA and 100 mM KCl. The same protocol was used for the purification of D2ΔC, D2-R1, D2-R2 and D2-R4. Ovine brain tubulin was purified by two cycles of assembly in a high-molarity buffer followed by disassembly (64). Before use, an additional cycle of assembly and disassembly was performed to remove inactive tubulin. SLD1, SLD1-R2 and SLD1-R3 were produced in *E. coli* and purified following established protocols (32).

**Crystallization and structure determination**. The SLD1:tubulin:D2-R3 ternary complex was prepared in 20 mM Mes-K, pH 6.8, 0.2 mM $MgCl_2$, 0.2 mM EGTA, by mixing the three proteins at a 1.5:1:1.5 stoichiometry ratio, respectively. It was then concentrated to about 250 µM and crystallized by vapor diffusion at 293 K in a buffer consisting of 20 to 25% (w/v) polyethylene glycol 3350 and 0.2 M K/Na tartrate. Crystals were harvested in the crystallization buffer containing also 20% glycerol and flash-cooled in liquid nitrogen. Crystals of SLD1:tubulin bound to D2-R1, D2-R2 or D2-R4, of tubulin:D2ΔC bound to SLD1-R3 or SLD1-R2, and of SLD1-R3:tubulin:D2-R3 were obtained similarly.

Datasets were collected at 100 K at the SOLEIL Synchrotron (PROXIMA-1 and PROXIMA-2A beamlines). They were processed with autoPROC (65), which implements the STARANISO treatment for anisotropy (66). Structures were solved by molecular replacement with Phaser (67) using SLD1:tubulin:D2 DARPin (pdb id 4F6R) as a search model, and refined with BUSTER (68) with iterative model building in Coot (69). Composite 2 $F_{obs}$-$F_{calc}$ electron

density omit maps were computed with Phenix (70). Data collection and refinement statistics for SLD1-R3:tubulin:D2-R3 are reported in Table S1. Figures of structural models were generated with PyMOL (https://www.pymol.org).

**Accession codes**. Coordinates and structure factors of SLD1-R3:tubulin:D2-R3 have been deposited with the Protein Data Bank with accession numbers 9F07.


## Acknowledgements

We thank M. Knossow (I2BC, Gif-sur-Yvette) for many useful discussions and for a critical reading of the manuscript. Diffraction data were collected at SOLEIL synchrotron (PROXIMA-1 and PROXIMA-2A beamlines, Saint-Aubin, France). We are most grateful to the machine and beam line groups for making these experiments possible. L.A.K. thanks the Université Paris-Saclay (doctoral school ED569) for PhD funding. This work has benefited from the crystallization platform of I2BC supported by French Infrastructure for Integrated Structural Biology (FRISBI) ANR-10-INBS-05. Financial support from the Agence Nationale de la Recherche (Grant ANR-22-CE11-0002-01 to B.G.) and from the CNRS through the MITI interdisciplinary programs is also acknowledged. In accordance with the open access conditions of the grants, the authors have applied a CC-BY public copyright license to any Author Accepted Manuscript version arising from this submission.


## References


1. Y. Wang, E. Mandelkow, Tau in physiology and pathology. *Nat Rev Neurosci* **17**, 5–21 (2016).
2. M. Goedert, M. G. Spillantini, R. Jakes, D. Rutherford, R. A. Crowther, Multiple isoforms of human microtubule-associated protein tau: sequences and localization in neurofibrillary tangles of Alzheimer's disease. *Neuron* **3**, 519–526 (1989).
3. I. Fischer, P. W. Baas, Resurrecting the mysteries of Big tau. *Trends Neurosci* **43**, 493–504 (2020).
4. D. C. Chung, *et al.*, The big tau splice isoform resists Alzheimer's-related pathological changes. [Preprint] (2024). Available at: https://www.biorxiv.org/content/10.1101/2024.07.30.605685v1 [Accessed 20 September 2024].
5. A. Himmler, D. Drechsel, M. W. Kirschner, D. W. Martin Jr., Tau consists of a set of proteins with repeated C-terminal microtubule-binding domains and variable N-terminal domains. *Mol Cell Biol* **9**, 1381–1388 (1989).
6. M. Goedert, D. S. Eisenberg, R. A. Crowther, Propagation of Tau aggregates and neurodegeneration. *Annu Rev Neurosci* **40**, 189–210 (2017).
7. Y. Shi, *et al.*, Structure-based classification of tauopathies. *Nature* **598**, 359–363 (2021).
8. S. Lövestam, *et al.*, Assembly of recombinant tau into filaments identical to those of Alzheimer's disease and chronic traumatic encephalopathy. *eLife* **11**, e76494 (2022).

9. G. Breuzard, *et al.*, Molecular mechanisms of tau binding to microtubules and its role in microtubule dynamics in live cells. *J Cell Sci* **126**, 2810–2819 (2013).
10. M. T. Gyparaki, *et al.*, Tau forms oligomeric complexes on microtubules that are distinct from tau aggregates. *Proc Natl Acad Sci USA* **118**, e2021461118 (2021).
11. R. Dixit, J. L. Ross, Y. E. Goldman, E. L. F. Holzbaur, Differential regulation of dynein and kinesin motor proteins by Tau. *Science* **319**, 1086–1089 (2008).
12. M. Ackmann, H. Wiech, E. Mandelkow, Nonsaturable binding indicates clustering of Tau on the microtubule surface in a paired helical filament-like conformation. *J Biol Chem* **275**, 30335–30343 (2000).
13. V. Siahaan, *et al.*, Kinetically distinct phases of tau on microtubules regulate kinesin motors and severing enzymes. *Nat Cell Biol* **21**, 1086–1092 (2019).
14. R. Tan, *et al.*, Microtubules gate tau condensation to spatially regulate microtubule functions. *Nat Cell Biol* **21**, 1078–1085 (2019).
15. V. Makrides, M. R. Massie, S. C. Feinstein, J. Lew, Evidence for two distinct binding sites for tau on microtubules. *Proc Natl Acad Sci USA* **101**, 6746–6751 (2004).
16. D. Janning, *et al.*, Single-molecule tracking of tau reveals fast kiss-and-hop interaction with microtubules in living neurons. *Mol Biol Cell* **25**, 3541–3551 (2014).
17. M. H. Hinrichs, *et al.*, Tau protein diffuses along the microtubule lattice. *J Biol Chem* **287**, 38559–38568 (2012).
18. S. Kar, J. Fan, M. J. Smith, M. Goedert, L. A. Amos, Repeat motifs of tau bind to the insides of microtubules in the absence of taxol. *EMBO J* **22**, 70–77 (2003).
19. J. Al-Bassam, R. S. Ozer, D. Safer, S. Halpain, R. A. Milligan, MAP2 and tau bind longitudinally along the outer ridges of microtubule protofilaments. *J Cell Biol* **157**, 1187–1196 (2002).
20. I. A. T. Schaap, B. Hoffmann, C. Carrasco, R. Merkel, C. F. Schmidt, Tau protein binding forms a 1 nm thick layer along protofilaments without affecting the radial elasticity of microtubules. *J Struct Biol* **158**, 282–292 (2007).
21. H. Kadavath, *et al.*, Tau stabilizes microtubules by binding at the interface between tubulin heterodimers. *Proc Natl Acad Sci USA* **112**, 7501–6 (2015).
22. A. R. Duan, *et al.*, Interactions between Tau and different conformations of tubulin: implications for Tau function and mechanism. *J Mol Biol* **429**, 1424–1438 (2017).
23. B. Gigant, *et al.*, Mechanism of Tau-promoted microtubule assembly as probed by NMR spectroscopy. *J Am Chem Soc* **136**, 12615–12623 (2014).
24. E. Kellogg, *et al.*, Near-atomic model of microtubule-tau interactions. *Science* **360**, 1242–1246 (2018).
25. R. L. Best, *et al.*, Tau isoform-specific stabilization of intermediate states during microtubule assembly and disassembly. *J Biol Chem* **294**, 12265–80 (2019).
26. C. Fauquant, *et al.*, Systematic identification of tubulin-interacting fragments of the microtubule-associated protein Tau leads to a highly efficient promoter of microtubule assembly. *J Biol Chem* **286**, 33358–33368 (2011).
27. H. Y. J. Fung, K. M. McKibben, J. Ramirez, K. Gupta, E. Rhoades, Structural characterization of Tau in fuzzy Tau:tubulin complexes. *Structure* **28**, 378-384.e4 (2020).
28. N. El Mammeri, A. J. Dregni, P. Duan, H. K. Wang, M. Hong, Microtubule-binding core of the tau protein. *Sci Adv* **8**, eabo4459 (2022).
29. K. A. Butner, M. W. Kirschner, Tau protein binds to microtubules through a flexible array of distributed weak sites. *J Cell Biol* **115**, 717–730 (1991).
30. H. Kadavath, *et al.*, The binding mode of a Tau peptide with tubulin. *Angew Chem Int Ed Engl* **57**, 3246–50 (2018).
31. M. Knossow, V. Campanacci, L. Ammar Khodja, B. Gigant, The mechanism of tubulin assembly into microtubules: insights from structural studies. *iScience* **23**, 101511 (2020).

32. I. Mignot, *et al.*, Design and characterization of modular scaffolds for tubulin assembly. *J Biol Chem* **287**, 31085–31094 (2012).
33. S. Lövestam, *et al.*, Disease-specific tau filaments assemble via polymorphic intermediates. *Nature* **625**, 119–125 (2024).
34. M. von Bergen, *et al.*, Assembly of τ protein into Alzheimer paired helical filaments depends on a local sequence motif ($^{306}$VQIVYK$^{311}$) forming β structure. *Proc Natl Acad Sci USA* **97**, 5129–5134 (2000).
35. N. Gustke, B. Trinczek, J. Biernat, E. M. Mandelkow, E. Mandelkow, Domains of tau protein and interactions with microtubules. *Biochemistry* **33**, 9511–9522 (1994).
36. D. M. Acosta, C. Mancinelli, C. Bracken, D. Eliezer, Post-translational modifications within tau paired helical filament nucleating motifs perturb microtubule interactions and oligomer formation. *J Biol Chem* **298**, 101442 (2022).
37. G. Lippens, B. Gigant, Elucidating Tau function and dysfunction in the era of cryo-EM. *J Biol Chem* **294**, 9316–25 (2019).
38. E. Prezel, *et al.*, Tau can switch microtubule network organizations: from random networks to dynamic and stable bundles. *Mol Biol Cell* **29**, 154–165 (2018).
39. P. Ganguly, *et al.*, Tau assembly: the dominant role of PHF6 (VQIVYK) in microtubule binding region repeat R3. *J Phys Chem B* **119**, 4582–4593 (2015).
40. A. P. Longhini, *et al.*, Precision proteoform design for 4R tau isoform selective templated aggregation. *Proc Natl Acad Sci USA* **121**, e2320456121 (2024).
41. R. Zhang, G. M. Alushin, A. Brown, E. Nogales, Mechanistic origin of microtubule dynamic instability and its modulation by EB proteins. *Cell* **162**, 849–859 (2015).
42. L. Qiang, *et al.*, Tau does not stabilize axonal microtubules but rather enables them to have long labile domains. *Curr Biol* **28**, 2181-2189.e4 (2018).
43. S. P. Maurer, F. J. Fourniol, G. Bohner, C. A. Moores, T. Surrey, EBs recognize a nucleotide-dependent structural cap at growing microtubule ends. *Cell* **149**, 371–382 (2012).
44. F. J. Fourniol, *et al.*, Template-free 13-protofilament microtubule–MAP assembly visualized at 8 Å resolution. *J Cell Biol* **191**, 463–470 (2010).
45. S. Ramirez-Rios, *et al.*, Tau antagonizes end-binding protein tracking at microtubule ends through a phosphorylation-dependent mechanism. *Mol Biol Cell* **27**, 2924–2934 (2016).
46. I. Hahn, *et al.*, Tau, XMAP215/Msps and Eb1 co-operate interdependently to regulate microtubule polymerisation and bundle formation in axons. *PLoS Genet* **17**, e1009647 (2021).
47. I. Tint, D. Jean, P. W. Baas, M. M. Black, Doublecortin associates with microtubules preferentially in regions of the axon displaying actin-rich protrusive structures. *J Neurosci* **29**, 10995–11010 (2009).
48. T. L. Hawkins, D. Sept, B. Mogessie, A. Straube, J. L. Ross, Mechanical properties of doubly stabilized microtubule filaments. *Biophys J* **104**, 1517–1528 (2013).
49. H. Inaba, *et al.*, Molecular encapsulation inside microtubules based on Tau-derived peptides. *Chem Eur J* **24**, 14958–14967 (2018).
50. F. Devred, *et al.*, Tau induces ring and microtubule formation from αβ-tubulin dimers under nonassembly conditions. *Biochemistry* **43**, 10520–10531 (2004).
51. E. M. Mandelkow, E. Mandelkow, R. A. Milligan, Microtubule dynamics and microtubule caps: a time-resolved cryo-electron microscopy study. *J Cell Biol* **114**, 977–991 (1991).
52. D. N. Drechsel, A. A. Hyman, M. H. Cobb, M. W. Kirschner, Modulation of the dynamic instability of tubulin assembly by the microtubule-associated protein tau. *Mol Biol Cell* **3**, 1141–1154 (1992).
53. D. Panda, J. C. Samuel, M. Massie, S. C. Feinstein, L. Wilson, Differential regulation of microtubule dynamics by three- and four-repeat tau: Implications for the onset of neurodegenerative disease. *Proc Natl Acad Sci USA* **100**, 9548–9553 (2003).

54. H. E. Feinstein, *et al.*, Oligomerization of the microtubule-associated protein tau is mediated by its N-terminal sequences: implications for normal and pathological tau action. *J Neurochem* **137**, 939–954 (2016).
55. A. Cario, S. P. Wickramasinghe, E. Rhoades, C. L. Berger, The N-terminal disease–associated R5L Tau mutation increases microtubule shrinkage rate due to disruption of microtubule-bound Tau patches. *J Biol Chem* **298**, 102526 (2022).
56. A. Fitzpatrick, *et al.*, Cryo-EM structures of tau filaments from Alzheimer's disease. *Nature* **547**, 185–90 (2017).
57. B. Falcon, *et al.*, Structures of filaments from Pick's disease reveal a novel tau protein fold. *Nature* **561**, 137–40 (2018).
58. W. Zhang, *et al.*, Novel tau filament fold in corticobasal degeneration. *Nature* **580**, 283–287 (2020).
59. B. L. Goode, M. Chau, P. E. Denis, S. C. Feinstein, Structural and functional differences between 3-repeat and 4-repeat Tau isoforms. *J Biol Chem* **275**, 38182–38189 (2000).
60. L. Pecqueur, *et al.*, A designed ankyrin repeat protein selected to bind to tubulin caps the microtubule plus end. *Proc Natl Acad Sci USA* **109**, 12011–12016 (2012).
61. S. Pernigo, A. Lamprecht, R. A. Steiner, M. P. Dodding, Structural basis for kinesin-1:cargo recognition. *Science* **340**, 356–359 (2013).
62. L. Pellegrini, *et al.*, Insights into DNA recombination from the structure of a RAD51–BRCA2 complex. *Nature* **420**, 287–293 (2002).
63. W. Wang, *et al.*, Insight into microtubule disassembly by kinesin-13s from the structure of Kif2C bound to tubulin. *Nat Commun* **8**, 70 (2017).
64. M. Castoldi, A. V. Popov, Purification of brain tubulin through two cycles of polymerization-depolymerization in a high-molarity buffer. *Protein Expr Purif* **32**, 83–88 (2003).
65. C. Vonrhein, *et al.*, Data processing and analysis with the autoPROC toolbox. *Acta Crystallogr Biol Crystallogr* **67**, 293–302 (2011).
66. I. J. Tickle, *et al.*, STARANISO (http://staraniso.globalphasing.org/cgi-bin/staraniso.cgi). Cambridge, United Kingdom: Global Phasing Ltd. (2018).
67. A. J. McCoy, *et al.*, Phaser crystallographic software. *J Appl Crystallogr* **40**, 658–674 (2007).
68. G. Bricogne, *et al.*, BUSTER version 2.10.4. Cambridge, United Kingdom: Global Phasing Ltd. (2017).
69. P. Emsley, B. Lohkamp, W. G. Scott, K. Cowtan, Features and development of Coot. *Acta Crystallogr Biol Crystallogr* **66**, 486–501 (2010).
70. D. Liebschner, *et al.*, Macromolecular structure determination using X-rays, neutrons and electrons: recent developments in Phenix. *Acta Crystallogr Biol Crystallogr* **75**, 861–877 (2019).